



## OPEN Plasma proteomics and lipidomics facilitate elucidation of the link between Alzheimer's disease development and vessel wall fragility

Suzumi M. Tokuoka<sup>1</sup>, Fumie Hamano<sup>1,2</sup>, Ayako Kobayashi<sup>1</sup>, Shungo Adachi<sup>3</sup>, Tomohiro Andou<sup>4</sup>, Tohru Natsume<sup>3</sup> & Yoshiya Oda<sup>1✉</sup>

Proximity Extension Assay (PEA) and mass spectrometry (MS) methodologies were utilized for the proteomic and lipidomic characterization of plasma specimens from patients who developed Alzheimer's disease. Proteomics was performed by both PEA and Liquid Chromatography (LC)/MS in this study, but all the more because LC/MS generally tends to be biased towards proteins with high expression and high variability, generating hypotheses proved challenging. Consequently, attempt was made to interpret the results from the PEA data. There were 150 significantly variable proteins and 68 lipids among 1000 proteins and 400 lipids. Pathway analysis was performed for both total and variable proteins measured to reduce bias, and it appeared that vascular fragility was related to AD. Furthermore, a multitude of lipid-associated proteins exhibited statistical changes. In certain instances, the function of individual proteins affected the factors associated with them, whereas others demonstrated trends contrary to anticipated outcomes. These trends seem indicative of diverse feedback mechanisms that provide homeostatic equilibrium. The degree of unsaturation of fatty acids, correlated with cardiovascular risk, warrants specific attention. Certain bile acids exhibited the potential to cause vascular endothelial damage. Contemplating these discoveries in tandem with previously documented phenomena, subtle shifts in homeostatic functions seem to be linked to the fragility of vascular endothelial cells. This is evidenced by the slow and chronic evolution of Alzheimer's disease from preclinical stages to its manifestation.

The increasing global prevalence of Alzheimer's disease (AD) stresses the critical necessity for developing efficacious therapeutic agents<sup>1</sup>. Despite numerous clinical trials, the success rate for AD pharmacotherapeutics remains disappointingly low (2% phase II and III success rate in 2003–2022)<sup>2</sup>, a predicament likely attributed to the reliance on animal models that only partially recapitulate AD pathology<sup>3</sup>. Since the advent of the inaugural transgenic mouse model in 1995, various AD models have been introduced; however, none comprehensively embody the entire spectrum of AD symptomatology<sup>4</sup>.

A critical impediment to the translational efficacy of these models may reside in their imprecise mimicry of human disease pathology<sup>5</sup>. Notably, sporadic AD typically manifests in humans when a person reaches his or her seventies, in stark contrast to the exceptionally early onset of AD-like symptoms in mouse models. This discrepancy, especially the prevalent use of relatively young mice in experimental paradigms, may tend to obscure accurate modeling of the disease<sup>6</sup>. The etiology of AD is inherently complex<sup>7</sup>, demanding a nuanced consideration of both genetic predispositions and environmental risk factors, and their molecular sequelae<sup>8</sup>.

<sup>1</sup>Department of Lipidomics, Graduate School of Medicine, The University of Tokyo, 7-3-1 Hongo, Bunkyo-ku, Tokyo 113-8654, Japan. <sup>2</sup>Life Sciences Core Facility, Graduate School of Medicine, The University of Tokyo, 7-3-1 Hongo, Bunkyo-ku, Tokyo 113-0033, Japan. <sup>3</sup>Cellular and Molecular Biotechnology Research Institute, National Institute of Advanced Industrial Science and Technology, 2-3-26 Aoumi, Koto-ku, Tokyo 135-0064, Japan. <sup>4</sup>Axcelead Drug Discovery Partners, Inc., 2-26-1 Muraoka-Higashi, Fujisawa, Kanagawa 251-0012, Japan. ✉email: yoda@m.u-tokyo.ac.jp

Reverse translational approaches, predicated on the analysis of human samples, yield more tangible insights by anchoring research in the empirical reality of clinical manifestations<sup>9</sup>. The heterogeneity intrinsic to human clinical data that result from individual variability frequently complicates constructing coherent conclusions<sup>10</sup>.

Yet, the synergistic integration of omics data with comprehensive patient health profiles is progressively facilitating more nuanced understandings of disease mechanisms and the corroboration of therapeutic targets<sup>11</sup>. Given the complexity and specificity of AD to humans, omics methodologies provide invaluable, unbiased datasets that elucidate the intricacies of the pathology involved<sup>12</sup>.

Proteomics would be a logical step because AD is a neurodegenerative disease<sup>13,14</sup> and is known to cause aggregation and deposition of proteins such as amyloid and tau. There have been several reports regarding AD plasma proteomics<sup>15–17</sup>, but many issues remain when using LC/MS, since only proteins with high expression levels, i.e. albumin, are detected. Moreover, reproducibility is poor and the number of samples that can be processed is reduced if albumin is removed in advance<sup>18,19</sup>.

The brain, a critical organ in the human body, possesses the second-highest lipid content after adipose tissue. Many reports have revealed that lipids—especially cholesterol, oxysterols, fatty acids, and phospholipids—are associated with AD. In recent year, lipidomics research has gained momentum in AD studies, particularly in identifying biomarkers for disease causation, prediction, diagnosis, and prevention<sup>20–22</sup>.

Multi-omics analyses afford far-ranging insights across a multitude of biological dimensions, encompassing genetic variability, environmental exposures, and the disease state itself; thereby catalyzing a generation of novel hypotheses<sup>23</sup>. Blood, by virtue of its systemic circulation throughout the body and the minimally invasive nature of its procurement, emerges as an exemplary medium for the elucidation of physiological and pathological states<sup>24</sup>. Accordingly, our study that covered more than 1000 plasma proteins and nearly 500 lipids proves that multi-omics analyses of human plasma samples greatly facilitate the determining of heterogeneity inherent in AD pathogenesis.

Results
Proteins altered in Alzheimer’s disease plasma

We utilized Proximity Extension Assay (PEA)<sup>25</sup> to quantify over 1000 plasma proteins because PEA can reproducibly quantify trace proteins present in plasma. We used PEA to measure 1161 protein molecules, and 911 proteins were detected from more than 90% of all samples. Of the 911 plasma proteins, 150 proteins exhibited significant variances both among the three clinical groups (AD, MCI, and CN) in a one-way ANOVA test following FDR multiple testing correction, and between AD and CN in Tukey’s HSD test (Supplementary Table 1).

We endeavored to determine impacted pathways by Reactome analyzing the differences (i.e., in enrichment)<sup>26</sup> between the pathways represented in the 911 proteins detected and in those 150 proteins which were significantly altered. It should be noted that proteins evaluated in the PEA panels are associated with specific biological functions, thus potentially introducing a certain degree of bias towards particular pathway information. Therefore, we calculated the degree of enrichment of those 150 proteins against the 911 proteins detected in PEA measurements (the second column from the right in Table 1) as a baseline, rather than against the Entities in the entire Reactome (rightmost column in Table 1). The proteins with substantial differences between AD and CN were predominantly linked to the pathways of “Platelet Activation, Signaling and Aggregation” and “Hemostasis,” implying a correlation between AD and vascular events. Additionally, various proteins associated with vascular damage and lipid metabolism demonstrated significant disparities in AD samples compared to those in CN samples.

Pathway identifier	Pathway name	Ratio of significantly different proteins divided by 911 proteins detected in analysis	Number of entities found in 150 of significantly different	Number of entities in 911 proteins detected in more than 90% of samples	Entities total number in reactome
R-HSA-76002	Platelet activation, signaling and aggregation	0.50	16	32	265
R-HSA-109582	Hemostasis	0.27	24	88	727
R-HSA-212436	Generic transcription pathway	0.25	15	60	1272
R-HSA-73857	RNA polymerase II transcription	0.25	15	60	1396
R-HSA-74160	Gene expression (transcription)	0.25	15	61	1568
R-HSA-5663202	Diseases of signal transduction by growth factor receptors and second messengers	0.24	15	62	483
R-HSA-9006934	Signaling by receptor tyrosine kinases	0.24	21	87	551
R-HSA-162582	Signal transduction	0.21	53	249	2606

Table 1. Pathway analysis by reactome. Pathways with more than 10 entities found in 150 protein exhibited significant differences between AD and NC, and the ratio of entities > 0.2 were shown. Reactome: https://curator.reactome.org/.

# Comparison PEA with liquid chromatography/mass spectrometry (LC/MS) proteomics

Proteomics by LC/MS was performed to verify the certainty of PEA. The results showed that 265 different proteins were detected by LC/MS, and 26 proteins were common to PEA. These common proteins correlated well with one another (Supplementary Table 2). Of the 150 proteins that were variable in PEA, only one protein was detectable in LC/MS, showing the same variability as in PEA. The repeatability of PEA was only 1.9% Coefficient Value (CV) (median), whereas LC/MS had a CV of 25% (median). LC/MS seemed to detect mainly proteins with high expression levels. Petrera et al. reported that LC/MS detected mainly highly expressed proteins and PEA detected low abundance proteins, and the number of proteins that could be detected in common by both was correlated<sup>25</sup>, and their results also support our data.

# Tissue inhibitor of metalloproteinases 4 and matrix metalloproteinase 9 in AD plasma

The protein with the lowest FDR p-value was the tissue inhibitor of metalloproteinases 4 (TIMP4) (Supplementary Table 1 and Fig. 1a). Notably, TIMP4 is known to increase and accumulate after vascular injury, playing a pivotal role in the proteolytic equilibrium of the damaged vasculature by inhibiting platelet matrix metalloproteinases (MMPs) and regulating platelet aggregation and recruitment<sup>27</sup>. Previous reports have highlighted an increase in TIMP4 in the blood of AD patients<sup>28,29</sup> and its potential role in suppressing the function of MMP-9<sup>30,31</sup>. Moreover, increased levels of MMP-9 in the blood have been linked to AD<sup>32</sup>. Such related research may corroborate our observations of a rise in MMP-9 levels in AD (Supplementary Table 1 and Fig. 1b). TIMP-4 has been suggested to be also involved in angiogenesis by a mechanism independent of MMP inhibition. Therefore, the present observation of elevated TIMP-4 in AD may not solely related to elevated MMPs but may related to several other pathways.

# Phospholipase A2 Group X and phospholipid profile

The protein with the second-lowest FDR p-value was Phospholipase A2 Group X (PLA2G10) (Fig. 1c). PLA2 enzymes cleave fatty chains of glycerophospholipids at the sn-2 position within cell membranes, and the PLA2G10 enzyme demonstrates a heightened propensity for severing polyunsaturated fatty acids (PUFAs)<sup>33</sup>. Accordingly, our phospholipid profiling revealed that phosphatidylcholines (PC) and phosphatidylethanolamines (PE) containing PUFA were significantly lower in AD samples (Fig. 2 and Supplementary Table 3). Therefore, we analyzed the correlation between phospholipid profile and PLA2G10 protein. Several PEs with high PUFA

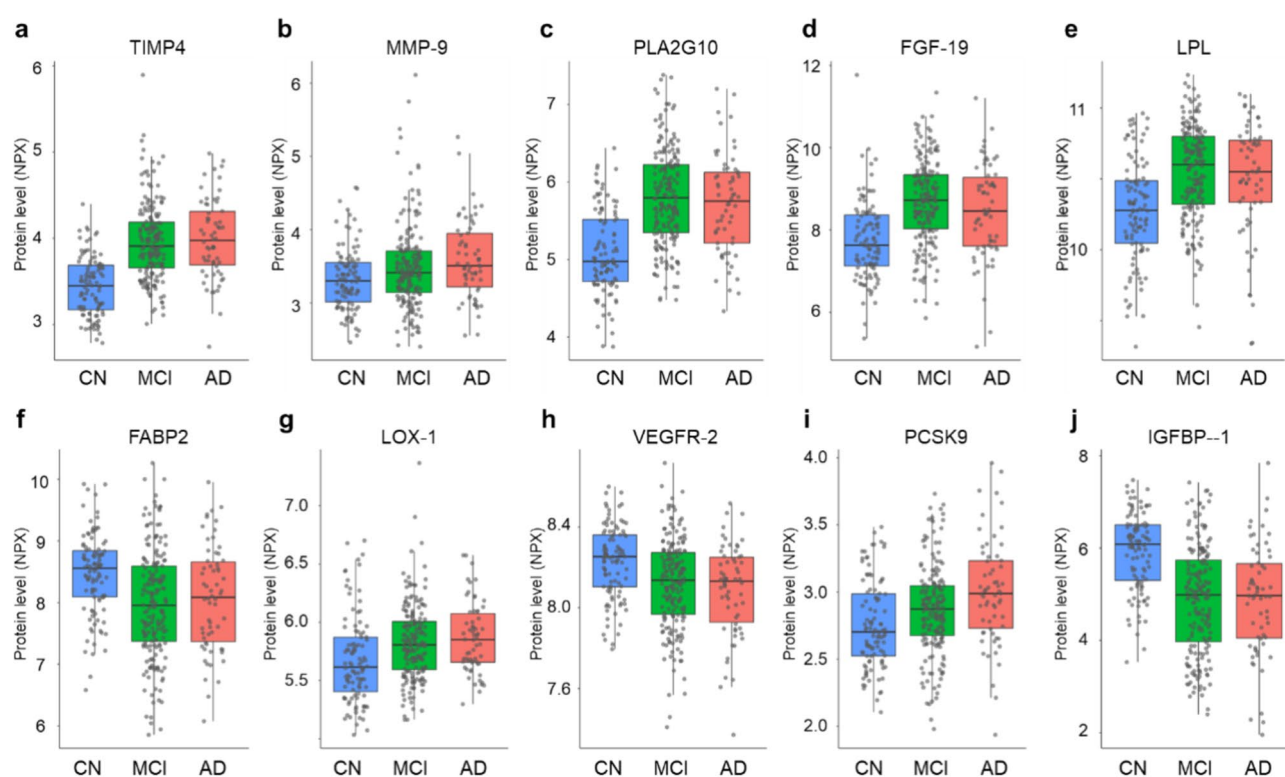


**Fig. 1.** Vessel wall event-related proteins and lipid metabolism-related proteins fluctuated in Alzheimer's disease. Level of proteins TIMP4 (a), MMP-9 (b), PLA2G10 (c), FGF-19 (d), LPL (e), FABP2 (f), LOX-1 (g), VEGFR-2 (h), PCSK9 (i), IGFBP-1 (j) in plasma samples. Those proteins exhibited significant variances in a one-way ANOVA test following FDR multiple testing correction and between AD and NC in Tukey's HSD test. See Supplementary Table 1 for the list of proteins. Horizontal lines in the rectangle represent the median, boxes represent the interquartile range, and whiskers represent the 5th and 95th percentiles. The dots represent each data point.

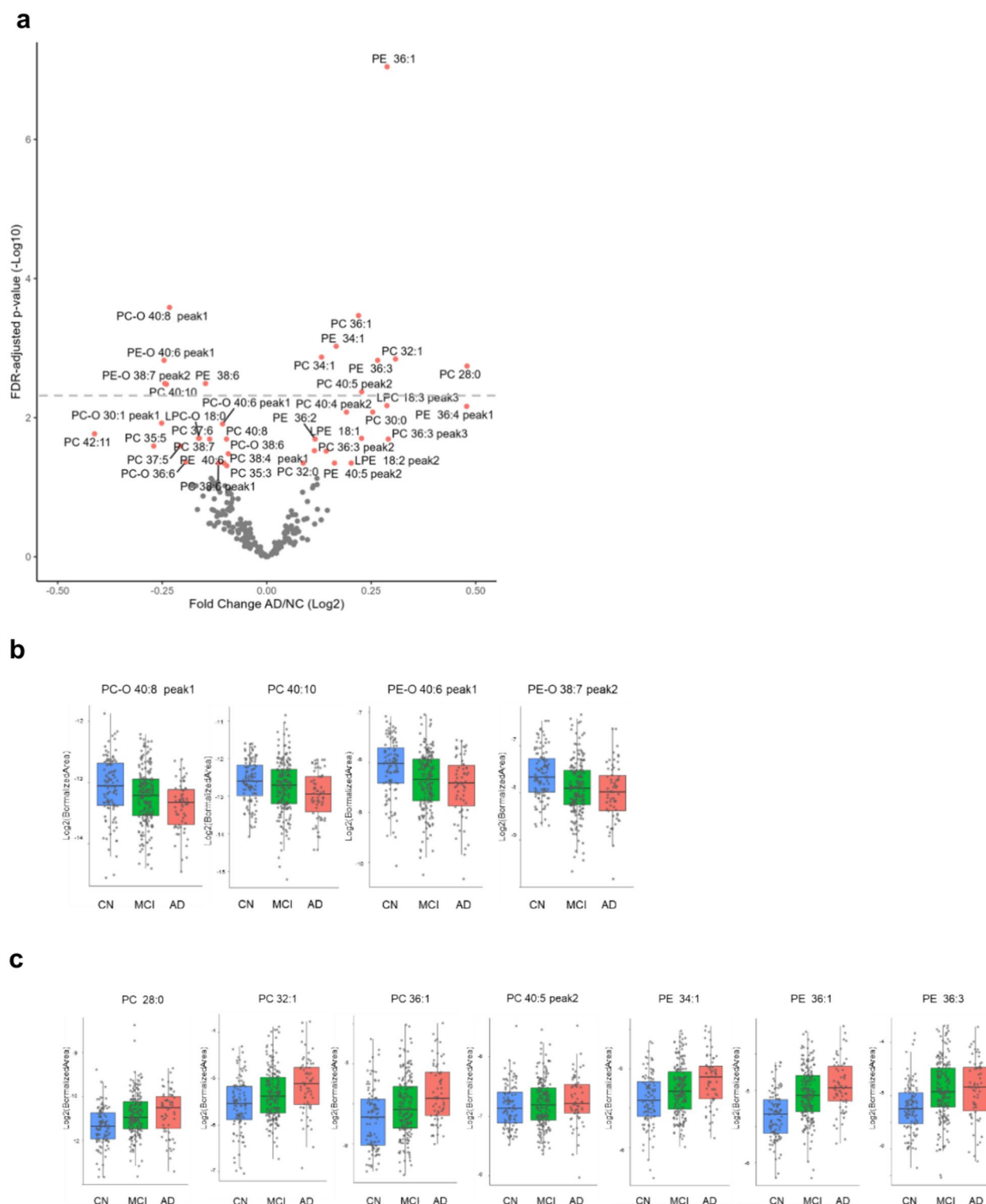


**Fig. 2.** Phospholipid profile differed between AD and control plasma. **(a)** Volcano plot for 216 phospholipids includes 180 PC and 36 PE features. The red dots represent the 39 phospholipids with significant differences (Student's *t*-test, FDR-adjusted *p*-value < 0.05). Phospholipids with low values in AD plasma samples were predominantly characterized as highly unsaturated ether lipids. See Supplementary Table 3 for the list of the phospholipids with significant differences. Measurements were performed at lipid Species Level; and when multiple peaks were detected, numbers were added from the earliest RT. Box plots **(b,c)** show the representative PC and PE species with significant difference in volcano plot (FDR-adjusted *p*-value < 0.005). Y axis showed log<sub>2</sub> scale for the normalized area expressed as a ratio to the total PC or PE peak area. Horizontal lines in the rectangle represent the median, boxes represent the interquartile range, and whiskers represent the 5th and 95th percentiles. The dots represent each data point.

content tended to show a negative correlation with PLA2G10 levels (Supplementary Table 4, Supplementary Fig. 1). This aligns with the anticipated functional capabilities of PLA2G10. Further analysis was extended to free fatty acids in the plasma samples. Among the 32 free fatty acids evaluated, the concentrations of seven fatty acids differed significantly between CN and AD (FDR < 0.05). Of special note, levels of the three omega-3 fatty acids DHA, DPA, and EPA were found to be lower in AD samples (Supplementary Table 5). It is not clear why these particular fatty acid are low levels in AD plasma with high PLA2G10 levels. One possibility is that the proportion of fatty acids used for lipid reconstitution may be decreasing, despite an increase in fatty acid excision from phospholipids by PLA2.

### Fibroblast growth factor-19 and bile acids

Fibroblast growth factor-19 (FGF-19) is secreted from the intestines and transported to the liver to activate fibroblast growth factor receptor 4 (FGFR4), thereby negatively regulating bile acid synthesis via suppression of cytochrome P450 7A1 (CYP7A1) expression<sup>34</sup>. Blood bile acid changes showed significant increases in deoxycholic acid (DCA), chenodeoxycholic acid (CDCA), glycodeoxycholic acid (GDCA), glycochenodeoxycholic acid (GCDCA), and hyocholic acid (HCA) in AD plasma compared to the CN samples (Fig. 3). The bile acids activating farnesoid X receptors (FXR) in the gastrointestinal tract provide a feedback mechanism whereby FXR activation leads to FGF-19 expression. Therefore, increased FGF-19 in AD (Fig. 1d) may be an attempt to inhibit the production of bile acids.

### Lipoprotein lipase and triglyceride

Lipoprotein lipase (LPL), an enzyme that hydrolyzes triglyceride fatty chains in lipoproteins, increased in AD samples (Fig. 1e). This study also assessed triglycerides (TG), discovering that 17 out of 37 measured triglycerides were significantly altered in AD samples compared to CN samples (FDR:  $p < 0.05$  with fold change < 0.8 or > 1.2) (Table 2). The TG species displaying elevated levels in AD samples were those with two or fewer double bonds in their total fatty chains. Conversely, five TG species, which were statistically lower in AD samples, possessed four or more double bonds. TG species consist of three fatty chains, with various isomers in their combinations. Molecular species-level measurements of TGs containing fatty chains with an unsaturation degree of four or higher are presented in Supplementary Fig. 2 as Box Plots. In AD samples, molecular species containing FA22:6, FA22:5, and FA20:5 decreased. MCI exhibited intermediate levels between CN and AD, whereas species containing FA20:4 showed no discernible trend (Supplementary Fig. 2c). To evaluate the differences in LPL levels among the three clinical groups are related to the observed TG change, the correlation between LPL levels and TG profiles was analyzed. LPL showed a weak negative correlation with the total TG area values and a weak positive correlation with some TG species; however, these were not the TG species changed in AD (Supplementary Table 6). Thus, the observed change in TG profiles is possibly caused by factors other than LPL level.

### Fatty acid binding protein 2

The fatty acid binding protein 2 (FABP2) expressed in intestinal cells is involved in the uptake and transport of fatty acids (FA) from the intestinal lumen to organelles within the cell. FABP2 binds saturated long-chain fatty acids with a high affinity, but binds with a lower affinity to unsaturated long-chain fatty acids. FABP2 is thought to prevent excessive accumulation of intracellular free FAs, especially saturated fatty acids (SFAs) thereby

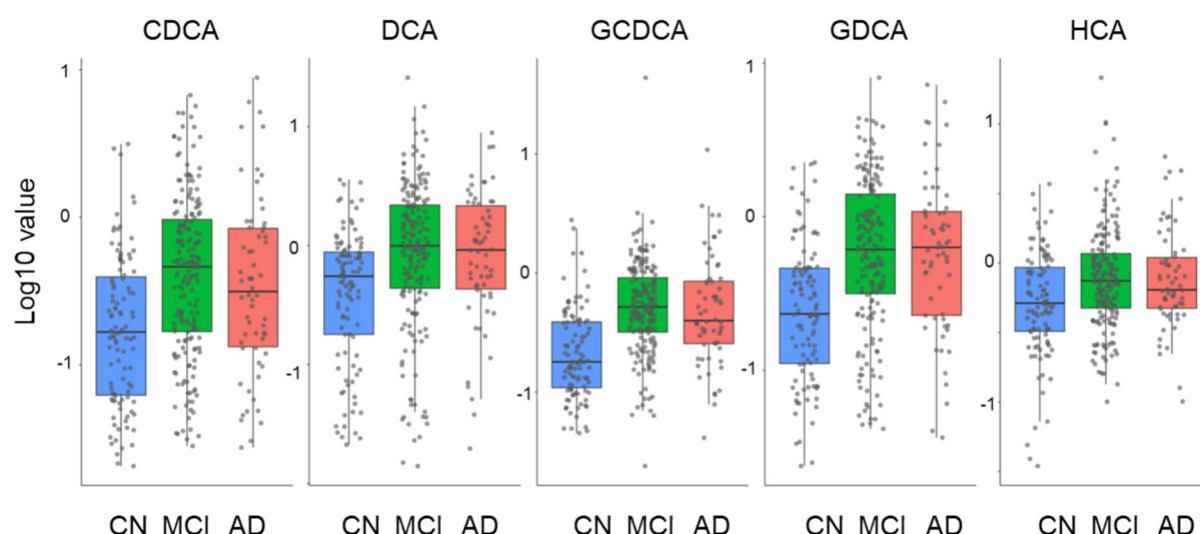


**Fig. 3.** Bile acids increased in AD plasma. Five bile acids out of eleven measured from plasma samples significantly increased in AD (Student's  $t$ -test, FDR-adjusted  $p$  value < 0.05). Bile acid levels are shown as arbitrary units converted to log10 using quality control values that are measured simultaneously. Horizontal lines in the rectangle represent the median, boxes represent the interquartile range, and whiskers represent the 5th and 95th percentiles. The dots represent each data point.



TG	Fold change (AD/CN)	FDR-adjusted p-value (BH)
TG 56:8	0.64	1.52E-05
TG 58:9	0.70	3.96E-03
TG 53:4	0.70	1.22E-05
TG 56:7	0.76	9.60E-04
TG 52:4	0.80	6.74E-08
TG 54:1	1.96	3.31E-06
TG 46:1	1.94	5.57E-06
TG 52:0	1.75	4.28E-06
TG 48:0	1.64	3.02E-06
TG 50:0	1.58	3.02E-06
TG 48:1	1.54	4.28E-06
TG 52:1	1.47	3.02E-06
TG 49:1	1.42	1.38E-03
TG 48:2	1.42	1.52E-05
TG 56:2	1.38	1.13E-02
TG 51:1	1.37	2.04E-03
TG 50:1	1.36	4.28E-06

**Table 2.** List of TG species with significant differences between AD and CN (Student's *t*-test, FDR-adjusted p value < 0.05, Fold Change < 0.8 or > 1.2).

maintaining free SFA concentrations at homeostatic levels and providing a protective function<sup>35</sup>. In AD, the observed lower levels of FABP2 (Fig. 1f) suggest a potential reduction in this protective function.

### Lectin-like oxidized LDL receptor-1 and vascular endothelial growth factor

Lectin-like oxidized LDL receptor-1 (LOX1), or oxidized low-density lipoprotein receptor 1 (OLR1), is associated with several diseases, including endothelial dysfunction and atherosclerosis<sup>36</sup>. An increase in LOX1 was observed in AD (Fig. 1g), indicating the likelihood of advanced atherosclerosis in AD patients. Activation of LOX1 by oxidized LDL (oxLDL) has been reported to increase the expression of various proangiogenic factors such as vascular endothelial growth factor (VEGF) and MMP-9<sup>37</sup>. Our data also show a significant decrease in VEGFR2 (Fig. 1h) accompanied with heightened levels of MMP-9 (Fig. 1b). A trend toward increased VEGFA and decreased VEGFR-3 was also observed (Supplementary Fig. 3).

### Proprotein Convertase Subtilisin/Kexin Type 9 (PCSK9) in AD blood and inflammation-associated proteins

Statistically increased levels of Proprotein Convertase Subtilisin/Kexin Type 9 (PCSK9) were detected in AD blood (Fig. 1i). PCSK9 binds to the LDL receptor and facilitates its degradation, potentially leading to an increase in LDL cholesterol in the bloodstream<sup>38</sup>. Both PCSK9 and LOX-1 are known to exacerbate during inflammatory responses<sup>39</sup>. Given their degree of elevation in our dataset, ongoing inflammation in AD can be inferred. The link between inflammation and AD has been extensively documented in numerous reports<sup>40,41</sup>. In relation to inflammation, four chemokines significantly increased in AD in this study (Supplementary Table 1 and Supplementary Fig. 4), all of which are associated with angiogenesis.

### Insulin-like growth factor binding protein 1

Insulin-like Growth Factor Binding Protein 1 (IGFBP-1) decreased in AD (Fig. 1j), and is a potential angiogenesis-related protein. The IGFBP-1 is believed to be instrumental in protecting and repairing vascular endothelial cells<sup>42–44</sup>. The diminished levels of IGFBP-1 in AD may suggest impaired repair functions of vascular endothelial cells, producing fragile vessel walls, and potentially increased cardiovascular disease risk. The IGFBP-1 is also a potential a risk factor for the development of glucose intolerance and insulin resistance<sup>45</sup>. To investigate the potential relationship between the observed changes in IGFBP-1 levels and glucose metabolism, the concentrations of glucose and glycolytic system-related molecules were evaluated. No significant difference was detected in the metabolites among the clinical groups (Supplementary Fig. 5).

### Apolipoproteins

Apolipoproteins play important roles for lipid transport and metabolism. Apolipoprotein E (APOE) polymorphism is the most common gene linked to late-onset Alzheimer's disease. Not only Apolipoprotein E, but also other apolipoproteins are linked to various diseases such as cardiovascular and neurodegenerative disease. Apolipoprotein M was the only apolipoprotein available by PEA detection and Apolipoprotein M level among clinical groups showed no statistical difference. Twelve peptides were detected for apolipoproteins by LC/MS proteomics with no statistical difference among clinical groups. The levels of Apolipoprotein M measured using PEA and

using LC/MS correlate very well ( $r=0.64$ ,  $p<0.01$ ), presumably indicating that both measurement techniques are reliable (Supplementary Fig. 6).

## Discussion

In this study, Reactome analysis of proteins that exhibited significant differences between AD and CN groups indicates a possible vascular association. Notably, several proteins with significant variations were linked to cardiovascular disease (CVD) risk. In CVD prevention and treatment, n-3 PUFAs are considered beneficial for cardiovascular health<sup>46</sup>. However, evidence supporting the role of n-3 PUFAs in cardiovascular prevention remains elusive<sup>47</sup>. Even if changing lipids can be found from lipidomics data, interpreting the results from lipidomics alone is a daunting task due to the lack of information on functions and poor lipid pathway maps. Therefore, the first step was to interpret the proteomics data and relate the lipid data. We focused on protein and lipid components that differ significantly between CN and AD. Interestingly, these components that we focused on, as shown in the BOX plots, are distributed over a wide range for much of the data in the MCI group, but the overall distribution of the data is between CN and AD or close to AD. This may be a remarkable point to focus on when considering the mechanism of the disease.

Several prospective studies have highlighted a correlation between SFA intake and the risk of cognitive impairment<sup>48,49</sup>. Fluctuations in bile acids (BAs) affect various metabolic regulation, including changes in lipid metabolism and absorption, and these fluctuations may trigger the onset of AD. Increased levels of BAs adversely affect vascular tone, endothelial function, arrhythmias, coronary atherosclerotic heart disease, heart failure, and other cardiovascular conditions<sup>50,51</sup>.

Additionally, studies suggest that the FABP2 (A54T) gene polymorphism may contribute to the development of CVD<sup>52</sup>. In elderly, 70 years of age or older, LPL and lipid homeostasis are linked to an atherosclerotic etiology of hemorrhagic and ischemic strokes or myocardial infarction<sup>53</sup>. The expression of PLA2G10 seems to inhibit atherosclerosis development<sup>54</sup>, though reports of both improvement and exacerbation of atherosclerosis<sup>33</sup>, and other conflicting data exist. This ambiguity extends to the association between PUFAs and CVD.

Increased MMP-9 levels post-stroke are associated with cognitive impairment<sup>55</sup> and contribute to the disruption of the brain-blood barrier (BBB)<sup>56</sup>. TIMP4 is also involved in lipid absorption<sup>57</sup>, impacting cholesterol metabolism and helping to prevent aortic plaque deposition<sup>58</sup>.

In advanced atherosclerosis, the expression of LOX-1 is noticeably upregulated in vascular cells. LOX-1, acting as a scavenger receptor for oxidized LDL (oxLDL)<sup>36</sup>, mediates the uptake of oxLDL into vascular cells, promoting foam cell formation and triggering atherosclerosis-promoting and fibrosis-promoting transcriptional programs<sup>59</sup>.

Insulin-like Growth Factor Binding Protein 1 (IGFBP-1) enhances endothelial regeneration and restores endothelial repair function<sup>44</sup>, providing a novel approach for preventing CVD under conditions like insulin resistance and diabetes mellitus<sup>42</sup>. IGFBP-1 levels increase with aging, possibly as an adaptive response to protect vascular endothelial cells against aging-related deterioration<sup>43</sup>. However, in our study, IGFBP-1 levels decreased in AD. This increased CVD risk may have worsened vascular dysfunction, conceivably related to AD.

The protein and lipid changes observed in this study represent not only the triggers and consequences of the onset of AD expressed in metabolites, but also the consequences of the human body's regulatory mechanisms that attempt to maintain homeostasis. For instance, decreases in DHA and DPA were accompanied by an increase in PLA2G10 possibly for elevating these fatty acids. An increase in bile acids led to heightened FGF-19 levels, likely as a compensatory mechanism for reducing bile acids. The increase in LPL was counterbalanced by the upregulation of ANGPTL3 to suppress LPL activity. Incorporating SFAs into TG reduces increased SFAs within cells. All of these are crucial for maintaining bodily physiological homeostasis.

In such a chronic disease as AD, homeostatic functions may gradually shift, leading to abnormal vascular function<sup>60,61</sup>. Many of the molecules that fluctuated in this study concern the vascular wall, and numerous studies suggest an association between AD and the fragility of the vessel wall<sup>62,63</sup>. It is posited that changes in vascular wall homeostasis and the failure of capillaries and other vessels may be instrumental in the early stages of AD progression. Particularly, disruption of the BBB is thought to contribute to be a contributory cause of cognitive decline<sup>64–66</sup>.

Combining the results of this study with previously reported phenomena allows for the conceptualization of a schematic representation of these changes (see Fig. 4). Vascular endothelial cells (VECs) are significantly altered in AD<sup>63,67,68</sup> and PUFAs such as DHA are easily oxidized, thereby weakening their protective effect on the vascular endothelium. Oxidized LDLs, generated by enzymatic or by non-enzymatic factors such as free radicals, cause further damage to the vascular endothelium. Increased several bile acids also contribute to endothelial damage. The reduction in FABP2 leads to the intracellular accumulation of SFAs, causing cellular toxicity. Vascular endothelial damage triggers the production of various chemokines and increases the number of factors related to angiogenesis, including VEGF.

Consequently, neurofilament light chain (NEFL), typically confined to the brain, becomes more likely to leak into the bloodstream, because the NEFL in plasma was significantly elevated in AD (Supplementary Table 1).

Recent reports indicate that vascular endothelial cell (EC) aging in AD is associated with reduced BBB function and angiogenesis in cerebrovascular vessels<sup>69</sup>, and that cerebrovascular structure is altered in AD<sup>63</sup>. We would like to emphasize that these reports were based on transcriptomics analysis of human brain samples, whereas our hypothesis is derived from proteomics and lipidomics of human plasma samples. It should be noted that both approaches are generally consistent with the aging and fragility of blood vessels occurring in early AD.

In this comprehensive study, we performed targeted proteomics using the PEA and targeted lipidomics using LC/MS on plasma samples from 352 elderly individuals. This analysis quantified an extensive array of more than 1000 proteins and nearly 400 lipids. The proteins that demonstrated significant alterations suggested a notable association between AD and vascular health or the lack thereof, with individual proteins appearing to correlate

## Correlation with AD

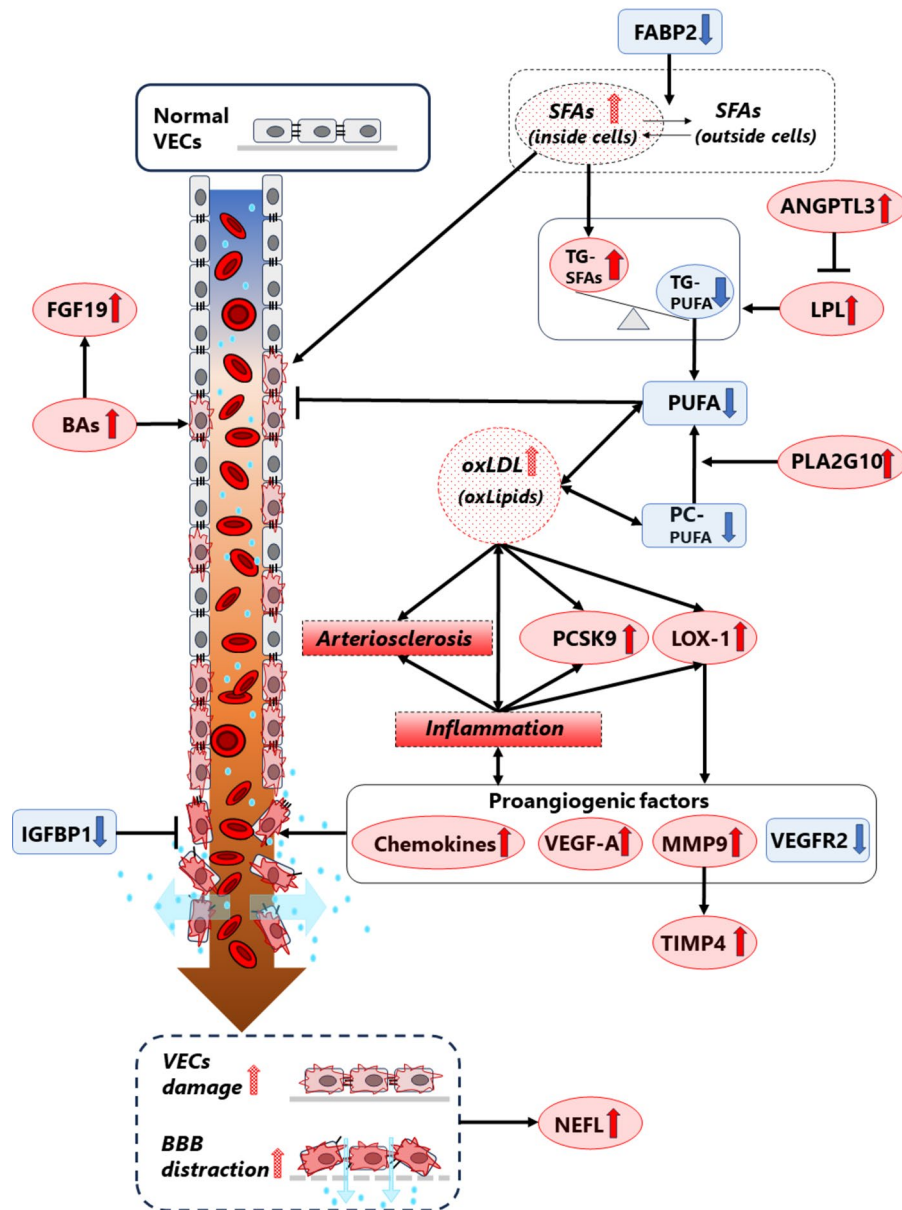


**Fig. 4.** Schematic representation of vascular endothelial cells (VECs) changes during AD development.

with CVD risk. Our data elucidate a highly provable correlation between AD and various lipid species, including PUFAs, saturated fatty acids, and bile acids. These findings collectively indicate that vascular function is likely compromised in AD, accompanied by the activation of feedback mechanisms aimed at maintaining physiological homeostasis. Whether vascular vessel wall fragility is a cause or a consequence of AD is unclear, and whether this hypothesis is AD-specific currently also remains uncertain. However, if this hypothesis is correct, therapy to correct vascular wall fragility may be therapeutic in a symptomatic way. Alternatively, we firmly believe that the development of a diagnostic method targeting the vulnerability of the vascular wall as an indicator may very well provide one objective measure of the progression of AD. AD progresses as a chronic condition, and the maintenance of vascular function homeostasis may gradually deteriorate, contributing to disease progression. Our study's results indicate that further research is needed to determine the specific relationships between vascular function and AD, or to identify AD-specific events. A comparative analysis of AD with other neurodegenerative diseases must be conducted to identify AD-specific phenomena and to further understand their unique pathophysiological characteristics.



Methods  
Demographic characteristics

Plasma samples from the biobank of the Japan National Center for Geriatrics and Gerontology (NCGG) were employed in this study. Participation in the NCGG Biobank was voluntary, and all participants completed informed consent in writing before registering. Sixty-two AD patients exhibited mild AD symptoms. Of the 62 patients 41 exhibited a Mini-Mental State Examination (MMSE) score of 23, and the remaining 21 exhibited an MMSE score of 22. In addition, the study included samples from 187 subjects diagnosed with mild cognitive impairment (MCI), and 103 subjects diagnosed as having been cognitively normal (CN) for at least 1 year after blood sampling (Table 3). We included CNs who had normal cognitive functions for a minimum of 1 year after the blood sample was taken. For AD, only mild AD patients with MMSE scores of 22–23 were considered. However, in the case of mild AD relying on MMSE scores without imaging data (and other detailed information), the borderline with MCI is often blurred and overlapping. An increase in AD compared to CN, if reduced by MCI, would not only complicate the interpretation of the results, but may also make the data insufficiently reliable. We therefore attempted to interpret the results by ensuring that the directionality of MCI and AD compared to CN was the same, or at least not contradictory.

Reagents

LC/MS grade acetonitrile, 2-propanol, HPLC-grade formic acid, and ammonium formate, sodium chloride, and 1-buthanol of Wako special grade, along with Wako 1st Grade ammonium hydrogencarbonate (FUJIFILM Wako Pure Chemical Corp., Osaka, Japan) were utilized.

The Aminoxyl TMT sixplex Label Reagent (Thermo Fisher Scientific Inc., Waltham, MA, USA), the coupling reagent 4-(4,6-Dimethoxy-1,3,5-triazin-2-yl)-4-methylmorpholinium Chloride (DMTMM) and 4-methylmorpholine (NMM) (Sigma-Aldrich Co., St. Louis, MO, USA), and 1-Ethyl-3-[3-Dimethylaminopropyl]carbodiimide hydrochloride (EDC) (Fuji Film Wako Pure Chemical Co.) were used for derivatization.

Ultrapure water was prepared using the Milli-Q system (Millipore, Billerica, MA, USA).

Human plasma samples and quality control sample

Ethical approval for this research was obtained from the Ethics Committee of the University of Tokyo Hospital, in strict compliance with pertinent university, local, and national guidelines and regulatory standards. The study received approval under the identification numbers 2019022NI and 2020033G, as sanctioned by the Institutional Research Ethics Committee of the Faculty of Medicine at The University of Tokyo. To control for the possibility of systematic errors caused by the order of the measurements, the samples in each group were intermixed and given a consecutive number before measurement. For quality control of inter-plate variation in the PEA proteomics, pooled samples made with all 352 plasma samples from NCGG in the set of the present study were used. For quality control in LC/MS/MS analysis, a stocked a pooled sample consisting of randomly selected 300 serum samples<sup>70</sup> was utilized.

PEA for proteomics

Plasma protein levels were measured using the PEA technology. This technology, provided by Olink Proteomics (Uppsala, Sweden), is a sensitive and specific method for protein quantification that uses pairs of antibody-conjugated oligonucleotides to detect proteins in biological samples.

The thirteen panels, CARDIOMETABOLIC, CARDIOVASCULAR II, III, CELL REGULATION, DEVELOPMENT, IMMUNE RESPONSE, INFLAMMATION, METABOLISM, NEUROLOGY, NEUROEXPLORATORY, ONCOLOGY II, ORGAN DAMAGE, and ONCOLOGY III were used. One µl plasma samples were used for each panel assay.

For the quantification process, the Fluidigm Biomark™ HS system was used for real-time quantitative PCR (qPCR) analysis. Data were processed with the Olink NPX manager software and transformed to Olink's NPX value, a relative protein quantification unit on a log2 scale. NPX values are derived from threshold cycle (Ct) values obtained through qPCR. Relative quantification is based on the comparative Ct method, employing Olink's built-in extension and inter-plate controls. The extension control consists of two oligonucleotides bound to the same antibody molecule, allowing for direct hybridization. During PCR amplification, all hybridized DNA oligonucleotides, including the extension control, are amplified at the same rate. Therefore, the resulting number of DNA amplicons represents a relative value to the initial concentration of the extension control in all samples. The Inter-plate Control (IPC) is a pooled sample containing 92 antibodies, each with a unique pair of DNA tags,

	CN	MCI	AD
Sample size	103	187	62
Female %	34	62	66.1
Age (years) Mean ± SD	73.9 ± 4.5	76.5 ± 5.9	75.7 ± 4.9
Age (years) Median	73	77	75
Age (years) Range	65–90	53–92	66–85

**Table 3.** Subject demographic characteristics. CN cognitively normal, MCI mild cognitive impairment, AD Alzheimer's disease.

and is included in triplicate on each plate. The median Ct value of these IPC triplicates is used to normalize each assay, compensating for potential variations between runs and plates.

The NPX value for each analyte is calculated as follows: First, the difference between the Ct value of the analyte and the extension control (dCtAnalyte) is determined. Next, the difference between dCtAnalyte and the inter-plate control (ddCtAnalyte) is calculated. Finally, a pre-determined correction factor, established by Olink during panel validation, is subtracted from ddCtAnalyte to obtain the NPX value for the analyte (NPXAnalyte). This correction factor inverts the scale, ensuring higher values correspond to stronger signals, and adjusts background levels to approximate zero.

To further clarify, no specific proteins were used as a baseline in our study. Instead, the relative quantification is based on the comparative Ct method using extension and inter-plate controls. Additionally, the values were not normalized to 1  $\mu$ L of blood but rather to the internal and inter-plate controls included in the Olink assay.

### LC/MS for proteomics

1  $\mu$ L of plasma samples was precipitated with TCA. Precipitated proteins were redissolved in guanidine hydrochloride. After reduction with TCEP and alkylation with iodoacetamide, it was digested with lysyl endopeptidase and trypsin. Resulting peptides were analyzed using an Evosep One LC system (EVOSEP) coupled to a Q-Exactive HF-X mass spectrometer (Thermo Scientific, Waltham, MA). Mobile phase A consisted of 0.1% formic acid/water, and mobile phase B consisted of 0.1% formic acid/acetonitrile. The analysis was conducted in data-dependent acquisition mode, selecting the top 25 mass spectrometry spectra between 380 and 1500 m/z for recording. All MS/MS spectra were searched against the protein sequences from the human NCBI Refseq database using Proteome Discoverer 2.2 with the SEQUEST search engine. The false discovery rate (FDR) for peptide spectrum matches was set to 1%.

### Lipid extraction

For measurements of PC, PE and TG, lipid extraction from plasma was done by adding 490  $\mu$ L of 2-propanol onto each 10  $\mu$ L of plasma sample, followed by a 15-s vortex at room temperature and stored at  $-30^{\circ}\text{C}$  for two hours. A 15-s vortex at room temperature again before centrifugation at 10,000 $\times$ g for 10 min at  $4^{\circ}\text{C}$ . 350  $\mu$ L of supernatant was collected and stored at  $-80^{\circ}\text{C}$  until use. These samples were used at their original concentration for TG measurements and diluted twofold with 2-propanol for phospholipid measurements. For the measurements of free fatty acids and bile acids, extraction by 1-butanol was performed followed by derivatization as described previously<sup>66</sup>.

### LC-MRM-MS for wide-targeted lipidomics

For PC and PE measurements, LCMS-8060 triple quadrupole mass spectrometers equipped with Nexera UHPLC (Shimadzu Co., Kyoto, Japan) were used. Shimadzu LabSolutions LCMS software version 5.9 (Shimadzu Co.) was used for instrument operation. ACQUITY UPLC BEH C8 columns (2.1 mm  $\times$  100 mm, 1.7  $\mu$ m) (Waters Co., Milford, MA, USA) was utilized for reversed-phase chromatography. The LC/MS method has previously been published<sup>70</sup>. The MRM transitions:  $[\text{M}+\text{H}]^{+} \rightarrow 184.05$  for PC (collision energy  $-33\text{ V}$ ) and  $[\text{M}+\text{H}]^{+} \rightarrow [\text{M}+\text{H}-141]^{+}$  (collision energy  $-23\text{ V}$ ) for PE were used. PC and PE possessing carbon chains 14–22 carbons in length in sn-1 and sn-2 were targeted. These transitions utilize fragmentation for polar head groups in phospholipids. Although highly sensitive, the composition of the two fatty chains is not determined by this MRM, so phospholipid names are expressed in terms of the lipid class and the sum of carbon atoms and the sum of double bond equivalents of the two fatty chains. When several separated peaks were observed from the same MRM transition, they were named peak1, peak2, and peak3, starting from the peak with the fastest retention time. The list of MRM transitions for PC and PE is shown in Supplementary Table 7. Peak areas were calculated by Traces software<sup>71</sup>. Peak areas were summed for each PC and PE class, and the peak areas of individual PC and PE species were then expressed as a ratio to the total class area. For quality control (QC) in LC/MS/MS analysis, a stocked a pooled sample consisting of randomly selected 300 serum samples was utilized. The QC measurements were performed every 11 samples, and only PC and PE species that met the criteria of a CV value within 30% for a total of 32 times QC measurements were used as the final data.

For TG measurements, LCMS-8040 triple quadrupole mass spectrometers equipped with Nexera UHPLC (Shimadzu Co.) were used. Shimadzu LabSolutions LCMS software version 5.9 (Shimadzu Co.) was used for instrument operation. Shim-pack Velox C18 (2.1  $\times$  50 mm, 2.7  $\mu$ m) (Shimadzu Co.) was utilized for reversed-phase chromatography. The flow rate was 0.4 mL/min, and the column temperature was  $45^{\circ}\text{C}$ . Mobile phase A consisted of 20 mM  $\text{NH}_4\text{HCO}_2$ /water, and mobile phase B consisted of 20% acetonitrile and 80% IPA. The pump gradient was programmed as follows: [time (%A/%B)]: from 0 min (85/15) to 0.1 min (85/15), to 8.4 min (95/5), 9 min (95/5), 9.1 min (85/15), 11 min (85/15). The parameters for the mass spectrometer were set as follows: nitrogen gas used as a nebulizer was set at 2.5 L/min, and drying gas was set at 10 L/min. Argon gas was used for collision-induced dissociation. Heat block temperature was set at  $400^{\circ}\text{C}$ , and desolvation line temperature was set at  $250^{\circ}\text{C}$ . The injection volume was 4  $\mu$ L. The list for MRM transitions for TG is shown in Supplementary Table 8. The transition list was developed for TG molecular species that can be reproducibly measured in human blood samples by performing some preliminary experiments. Peak areas were calculated by Traces software<sup>71</sup>. In the transitions, Q1 was set as the parent ion of the ammonium adduct and Q3 as the neutral loss (NL) of a fatty chain. Thus, the fatty acyl chain components of the TG can be observed with their respective NL ions. The species-level TG name is expressed as the sum of carbon atoms and the sum of double bond equivalents of the three fatty chains. The species-level TG signal values were calculated as the sum of area values of the MRM transition peak with the same Q1 transitions. For quality control (QC) in LC/MS/MS analysis, a stocked a pooled sample consisting of randomly selected 300 serum samples<sup>71</sup> was utilized. The QC measurements were

performed every 11 samples, and only peaks that met the criteria of a CV value within 30% for a total of 32 times of QC measurements were used as the final data. Peak areas for each TG species were summed for total TG area in each sample, and the peak areas of individual TG species were then expressed as a ratio to the total TG area.

For free fatty acid and bile acid measurements, tandem mass tag (TMT) derivatization was carried out utilizing aminoxy TMT sixplex Label Reagent. The derivatization procedures and LC/MS method have been previously described<sup>70</sup>. MRM transitions:  $[M-H+303.25] + \rightarrow 126.15, \rightarrow 127.15, \rightarrow 128.15, \rightarrow 129.15, \rightarrow 130.15$ , and  $\rightarrow 131.15$ , were used for each reporter ion. Targeted fatty acid in these measurements were those of carbon numbers 12 to 24. Targeted bile acids in these measurements were colic acid (CA), chenodeoxycholic acid (CDCA), deoxycolic acid (DCA), glycocholic acid (GCA), glycochenodeoxycholic acid (GCDCA), glycodeoxycholic acid (GDCA), glycohyodeoxycholic acid (GHDCA), glyoursodeoxycholic acid (GUDCA), hyocholic acid (HCA), isolithocholic acid (isoLCA), lithocholic acid (LCA), and ursodeoxycholic acid (UDCA). The list for MRM transitions for this analysis is shown in Supplementary Table 9. Peak areas were calculated by Traces software<sup>71</sup>. For quality control (QC) in this analysis, a stocked a pooled sample consisting of randomly selected 300 serum samples were utilized. As described previously<sup>70</sup>, the data for each fatty acid or bile acid species were expressed as the ratio to the signal of QC samples that were analyzed in the same injection in this multiplex assay.

### LC/MS and gas chromatography (GC)/MS for metabolomics

For metabolite measurements by LC/MS, 5500QTRAP mass spectrometer (AB Sciex Pty. Ltd., Toronto, Canada) equipped with Nexera UHPLC (Shimadzu Co.) were used. ZIC-cHILIC column ( $2.1 \times 100$  mm,  $3 \mu\text{m}$ ; Merck Millipore) was utilized. The flow rate was  $0.4 \text{ mL/min}$ , and the column temperature was  $30^\circ\text{C}$ . Mobile phase A consisted of  $10 \text{ mM}$  ammonium formate/water, and mobile phase B consisted of acetonitrile. For metabolite measurements by GC/MS, dried samples were derivatized by oximation and trimethylsilylation. The derivatized metabolites were then injected into an Agilent 7890A series gas chromatography system. Chromatographic separation was performed in a J&W Scientific DB-5MS-DG column ( $30 \text{ m} \times 0.25 \text{ mm i.d.}$ ,  $\text{df} = 0.25 \mu\text{m}$ ; Agilent Technologies Inc., Santa Clara, CA) by a temperature gradient with helium gas flow at a rate of  $1 \text{ mL/min}$ . Eluted metabolites were introduced into an Agilent 7010B triple quadrupole mass spectrometer for electron impact ionization and scanned in MRM mode. MRM peak areas were calculated and relative comparisons were made between each sample to pooled QC samples.

### Data processing, statistics

For LC/MS lipidomics, the chromatogram peaks of area under curve (AUC) values were exported from TRACES<sup>71</sup>; and area ratio and CV for QC were analyzed using Microsoft Excel or R software (version 4.2.1). One-way ANOVA (for Supplementary Table 1) was performed using MetaboAnalyst 5.0 software<sup>72</sup>, with missing value treatment that used one-fifth of the lowest value. Student's t-test with the multiple testing adjusting of p-values obtained by the Benjamini–Hochberg method was conducted by R software (for Figs. 2, T 3, Table 2, Supplementary Table 3, Supplementary Table 5, Supplementary Table 6). Spearman's correlation analysis was performed with R software e (for Supplementary Fig. 1, Supplementary Figs. 6, Supplementary Table 4, Supplementary Table 6). The volcano plot was drawn by R software.

### Data availability

All data supporting the findings of this study are available at <https://lipidomics.m.u-tokyo.ac.jp/repos/tokuoka/20240426.zip>.

Received: 30 April 2024; Accepted: 23 August 2024

Published online: 27 August 2024

### References

- Cummings, J. et al. Alzheimer's disease drug development pipeline: 2023. *Alzheimer's Dementia Transl. Res. Clin. Interv.* **9**, e12385 (2023).
- Kim, C. K. et al. Alzheimer's disease: Key insights from two decades of clinical trial failures. *J. Alzheimers Dis.* **87**, 83–100 (2022).
- Drummond, E. et al. Potential novel approaches to understand the pathogenesis and treat Alzheimer's disease. *J. Alzheimers Dis.* **64**, S299–S312 (2018).
- McKean, N. E., Handley, R. R. & Snell, R. G. A review of the current mammalian models of Alzheimer's disease and challenges that need to be overcome. *Int. J. Mol. Sci.* **22**, 13168 (2021).
- King, A. The search for better animal models of Alzheimer's disease. *Nature* **559**, S13–S15 (2018).
- Jucker, M. The benefits and limitations of animal models for translational research in neurodegenerative diseases. *Nat. Med.* **16**, 1210–1214 (2010).
- Neff, E. P. Animal models of Alzheimer's disease embrace diversity. *Lab Anim.* **48**, 255–259 (2019).
- Fisher, E. M. C. & Bannerman, D. M. Mouse models of neurodegeneration: Know your question, know your mouse. *Sci. Transl. Med.* **11**, eaaq1818 (2019).
- Kasichayanula, S. & Venkatakrishnan, K. Reverse translation: The art of cyclical learning. *Clin. Pharmacol. Ther.* **103**, 152–159 (2018).
- Shakhnovich, V. It's time to reverse our thinking: The reverse translation research paradigm. *Clin. Transl. Sci.* **11**, 98–99 (2018).
- Wagner, J. A. Patient-centered reverse translation. *Clin. Pharmacol. Ther.* **103**, 168–170 (2018).
- Wniewski, T. & Drummond, E. *Future Horizons in Alzheimer's Disease Research. Progress in Molecular Biology and Translational Science* Vol. 168 (Elsevier Inc., 2019).
- Rayaprolu, S. et al. Systems-based proteomics to resolve the biology of Alzheimer's disease beyond amyloid and tau. *Neuropsychopharmacology* **46**, 98–115 (2021).
- Moya-Alvarado, G., Gershoni-Emek, N., Perlson, E. & Bronfman, F. C. Neurodegeneration and Alzheimer's disease (AD), what can proteomics tell us about the Alzheimer's brain?. *Mol. Cell Proteomics* **15**, 409–425 (2016).
- Jaeger, P. A. et al. Network-driven plasma proteomics expose molecular changes in the Alzheimer's brain. *Mol. Neurodegener.* **11**, 31 (2016).

16. Pernecky, R. & Guo, L. H. Plasma proteomics biomarkers in Alzheimer's disease: Latest advances and challenges. *Methods Mol. Biol.* **1303**, 521–529 (2016).
17. Guo, L. H., Alexopoulos, P., Wagenpfeil, S., Kurz, A. & Pernecky, R. Alzheimer's disease neuroimaging initiative. Plasma proteomics for the identification of Alzheimer disease. *Alzheimer Dis. Assoc. Disord.* **27**, 337–342 (2013).
18. Palström, N. B., Rasmussen, L. M. & Beck, H. C. Affinity capture enrichment versus affinity depletion: A comparison of strategies for increasing coverage of low-abundant human plasma proteins. *Int. J. Mol. Sci.* **21**, 5903 (2020).
19. Pringels, L., Broeckx, V., Boonen, K., Landuyt, B. & Schoofs, L. Abundant plasma protein depletion using ammonium sulfate precipitation and Protein A affinity chromatography. *J. Chromatogr. B Analyt. Technol. Biomed. Life Sci.* **1089**, 43–59 (2018).
20. Kalli, E. Nutritional lipidomics in Alzheimer's disease. *Adv. Exp. Med. Biol.* **1195**, 95–104 (2020).
21. Cuperlovic-Culf, M. & Badhwar, A. Recent advances from metabolomics and lipidomics application in Alzheimer's disease inspiring drug discovery. *Expert Opin. Drug Discov.* **15**, 319–331 (2020).
22. Wong, M. W., Braid, N., Poljak, A. & Sachdev, P. S. The application of lipidomics to biomarker research and pathomechanisms in Alzheimer's disease. *Curr. Opin. Psychiatry* **30**, 136–144 (2017).
23. Dong, X., Liu, C. & Dozmorov, M. Review of multi-omics data resources and integrative analysis for human brain disorders. *Brief Funct. Genomics* **20**, 223–234 (2021).
24. Yurkovich, J. T. & Hood, L. Blood is a window into health and disease. *Clin. Chem* **65**, 1204–1206 (2019).
25. Petrer, A. et al. Multiplatform approach for plasma proteomics: Complementarity of Olink proximity extension assay technology to mass spectrometry-based protein profiling. *J. Proteome Res.* **20**, 751–762 (2021).
26. Rothfels, K. et al. Using the reactome database. *Curr. Protoc.* **3**, e722 (2023).
27. Radomski, A. et al. Identification, regulation and role of tissue inhibitor of metalloproteinases-4 (TIMP-4) in human platelets. *Br. J. Pharmacol.* **137**, 1330–1338 (2002).
28. Lindbohm, J. V. et al. Plasma proteins, cognitive decline, and 20-year risk of dementia in the Whitehall II and Atherosclerosis Risk in Communities studies. *Alzheimer's Demet.* **18**, 612–624 (2022).
29. Ehtewish, H. et al. Blood-based proteomic profiling identifies potential biomarker candidates and pathogenic pathways in dementia. *Int. J. Mol. Sci.* **24**, 8117 (2023).
30. Mishra, P. K., Metreveli, N. & Tyagi, S. C. MMP-9 gene ablation and TIMP-4 mitigate PAR-1-mediated cardiomyocyte dysfunction: A plausible role of dicer and miRNA. *Cell Biochem. Biophys.* **57**, 67–76 (2010).
31. Xing, Y. et al. Targeting interleukin-21 inhibits stress overload-induced cardiac remodeling via the TIMP4/MMP9 signalling pathway. *Eur. J. Pharmacol.* **940**, 175482 (2023).
32. Lorenzl, S. et al. Increased plasma levels of matrix metalloproteinase-9 in patients with Alzheimer's disease. *Neurochem. Int.* **43**, 191–196 (2003).
33. Murakami, M., Sato, H. & Taketomi, Y. Modulation of immunity by the secreted phospholipase A2 family. *Immunol. Rev.* **317**, 42–70 (2023).
34. Li, T. & Chiang, J. Y. L. Bile acid signaling in metabolic disease and drug therapy. *Pharmacol. Rev.* **66**, 948–983 (2014).
35. Gajda, A. M. & Storch, J. Enterocyte fatty acid-binding proteins (FABPs): Different functions of liver and intestinal FABPs in the intestine. *Prostaglandins Leukot. Essent. Fatty Acids* **93**, 9–16 (2015).
36. Chistiakov, D. A., Orekhov, A. N. & Bobryshev, Y. V. LOX-1-mediated effects on vascular cells in atherosclerosis. *Cell Physiol. Biochem.* **38**, 1851–1859 (2016).
37. González-Chavarría, I. et al. Lectin-like oxidized LDL receptor-1 is an enhancer of tumor angiogenesis in human prostate cancer cells. *PLoS ONE* **9**, e106219 (2014).
38. Spolitu, S., Dai, W., Zadroga, J. A. & Ozcan, L. Proprotein convertase subtilisin/kexin type 9 and lipid metabolism. *Curr. Opin. Lipidol.* **30**, 186–191 (2019).
39. Tam, J., Thankam, F., Agrawal, D. K. & Radwan, M. M. Critical role of LOX-1-PCSK9 axis in the pathogenesis of atheroma formation and its instability. *Heart Lung Circ.* **30**, 1456–1466 (2021).
40. Leonardo, S. & Fregni, F. Association of inflammation and cognition in the elderly: A systematic review and meta-analysis. *Front. Aging Neurosci.* **15**, 1069439 (2023).
41. Chai, Y. L. et al. Inflammatory panel cytokines are elevated in the neocortex of late-stage Alzheimer's disease but not Lewy body dementias. *J. Neuroinflammation* **20**, 111 (2023).
42. Rajwani, A. et al. Increasing circulating IGFBP1 levels improves insulin sensitivity, promotes nitric oxide production, lowers blood pressure, and protects against atherosclerosis. *Diabetes* **61**, 915–924 (2012).
43. Wu, X., Zheng, W., Jin, P., Hu, J. & Zhou, Q. Role of IGFBP1 in the senescence of vascular endothelial cells and severity of aging-related coronary atherosclerosis. *Int. J. Mol. Med.* **44**, 1921–1931 (2019).
44. Aziz, A. et al. Insulin-like growth factor-binding protein-1 improves vascular endothelial repair in male mice in the setting of insulin resistance. *Endocrinology* **159**, 696–709 (2018).
45. Haywood, N. J., Slater, T. A., Matthews, C. J. & Wheatcroft, S. B. The insulin like growth factor and binding protein family: Novel therapeutic targets in obesity and diabetes. *Mol. Metab.* **19**, 86–96 (2019).
46. Drenjančević, I. & Pitha, J. Omega-3 polyunsaturated fatty acids—vascular and cardiac effects on the cellular and molecular level (narrative review). *Int. J. Mol. Sci.* **23**, 2104 (2022).
47. Colussi, G., Catena, C., Novello, M., Bertin, N. & Sechi, L. A. Impact of omega-3 polyunsaturated fatty acids on vascular function and blood pressure: Relevance for cardiovascular outcomes. *Nutr. Metab. Cardiovasc. Dis.* **27**, 191–200 (2017).
48. Morris, M. C. & Tangney, C. C. Dietary fat composition and dementia risk. *Neurobiol. Aging* **35**, S59–S64 (2014).
49. Barnard, N. D., Bunner, A. E. & Agarwal, U. Saturated and trans fats and dementia: A systematic review. *Neurobiol. Aging* **35**, S65–S73 (2014).
50. Zhang, R. et al. Overview of bile acid signaling in the cardiovascular system. *World J. Clin. Cases* **9**, 308–320 (2021).
51. Zhang, B. C. et al. Increased serum bile acid level is associated with high-risk coronary artery plaques in an asymptomatic population detected by coronary computed tomography angiography. *J. Thorac. Dis.* **11**, 5063–5070 (2019).
52. Wanby, P., Palmquist, P., Rydén, I., Brattström, L. & Carlsson, M. The FABP2 gene polymorphism in cerebrovascular disease. *Acta Neurol. Scand.* **110**, 355–360 (2004).
53. Mekke, J. M. et al. Plasma lipoprotein lipase is associated with risk of future major adverse cardiovascular events in patients following carotid endarterectomy. *Eur. J. Vasc. Endovasc.* **65**, 700–709 (2023).
54. Ait-Oufella, H. et al. Group X secreted phospholipase a2 limits the development of atherosclerosis in LDL receptor-null mice. *Arterioscler. Thromb. Vasc. Biol.* **33**, 466–473 (2013).
55. Zhao, J. et al. Is matrix metalloproteinase-9 associated with post-stroke cognitive impairment or dementia?. *J. Integr. Neurosci.* **21**, 160 (2022).
56. Weekman, E. M. & Wilcock, D. M. Matrix metalloproteinase in blood-brain barrier breakdown in dementia. *J. Alzheimer Dis.* **49**, 893–903 (2015).
57. Sakamuri, S. S. V. P. et al. Absence of tissue inhibitor of metalloproteinase-4 (TIMP4) ameliorates high fat diet-induced obesity in mice due to defective lipid absorption. *Sci. Rep.* **7**, 1–13 (2017).
58. Hu, M. et al. Loss of TIMP4 (tissue inhibitor of metalloproteinase 4) promotes atherosclerotic plaque deposition in the abdominal aorta despite suppressed plasma cholesterol levels. *Arterioscler. Thromb. Vasc. Biol.* **41**, 1874–1889 (2021).



59. Ishiyama, J., Taguchi, R., Yamamoto, A. & Murakami, K. Palmitic acid enhances lectin-like oxidized LDL receptor (LOX-1) expression and promotes uptake of oxidized LDL in macrophage cells. *Atherosclerosis* **209**, 118–124 (2010).
60. Frere, S. & Slutsky, I. Alzheimer's disease: From firing instability to homeostasis network collapse. *Neuron* **97**, 32–58 (2018).
61. Styr, B. & Slutsky, I. Imbalance between firing homeostasis and synaptic plasticity drives early-phase Alzheimer's disease. *Nat. Neurosci.* **21**, 463–473 (2018).
62. Park, L. et al. The key role of transient receptor potential melastatin-2 channels in amyloid- $\beta$ -induced neurovascular dysfunction. *Nat. Commun.* **5**, 1–12 (2014).
63. Sun, N. et al. Single-nucleus multiregion transcriptomic analysis of brain vasculature in Alzheimer's disease. *Nat. Neurosci.* **26**, 970–982 (2023).
64. Sweeney, M. D., Sagare, A. P. & Zlokovic, B. V. Blood-brain barrier breakdown in Alzheimer disease and other neurodegenerative disorders. *Nat. Rev. Neurol.* **14**, 133–150 (2018).
65. Montagne, A. et al. APOE4 leads to blood–brain barrier dysfunction predicting cognitive decline. *Nature* **581**, 71–76 (2020).
66. Lee, R. L. & Funk, K. E. Imaging blood–brain barrier disruption in neuroinflammation and Alzheimer's disease. *Front. Aging Neurosci.* **15**, 1–8 (2023).
67. Custodia, A. et al. Endothelial progenitor cells and vascular alterations in Alzheimer's disease. *Front. Aging Neurosci.* **13**, 1–11 (2022).
68. Bryant, A. et al. Endothelial cells are heterogeneous in different brain regions and are dramatically altered in Alzheimer's disease. *J. Neurosci.* **43**, 4541–4557 (2023).
69. Tsartsalis, S. et al. A single nuclear transcriptomic characterisation of mechanisms responsible for impaired angiogenesis and blood-brain barrier function in Alzheimer's disease. *Nat. Commun.* **15**, 2243 (2024).
70. Tokuoka, S. M. et al. Development of tandem mass tag labeling method for lipid molecules containing carboxy and phosphate groups, and their stability in human serum. *Metabolites* **11**, 19 (2021).
71. Kita, Y. et al. TRACES: A lightweight browser for liquid chromatography-multiple reaction monitoring-mass spectrometry chromatograms. *Metabolites* **12**, 354 (2022).
72. Pang, Z. et al. Using MetaboAnalyst 5.0 for LC–HRMS spectra processing, multi-omics integration and covariate adjustment of global metabolomics data. *Nat. Protoc.* **17**, 1735–1761 (2022).

## Acknowledgements

We thank Junko Ikeda and Hiroki Nakae of Japan bio Measurement & Analysis Consortium (JAMC) for coordinating with related parties in conducting this study, and the National Center for Geriatrics and Gerontology (NCGG) Biobank for their invaluable contributions to collecting plasma samples. This research was supported by AMED (23ae0101077h0005) (to S.M.T. and T.N.), AMED (23ae0121041h0003) (to Y.O.) and JSPS KAKENHI (21K06853) (to S.M.T.). The Department of Lipidomics is supported by the Shimadzu Corporation. The funders had no role in the study design, data collection and analysis, decision to publish, or preparation of the manuscript.

## Author contributions

Y.O. and T.N. provided the concept, idea and experimental design for the studies. S.M.T., F.H., A.K., S.A. and T.A. collected and analyzed data. Y.O. and S.M.T. wrote the manuscript. Y.O. and S.M.T. analyzed and interpreted data and reviewed the manuscript. F.H. provided support for data interpretation.

## Competing interests

The authors declare no competing interests.

## Additional information

**Supplementary Information** The online version contains supplementary material available at <https://doi.org/10.1038/s41598-024-71097-9>.

**Correspondence** and requests for materials should be addressed to Y.O.

**Reprints and permissions information** is available at [www.nature.com/reprints](http://www.nature.com/reprints).

**Publisher's note** Springer Nature remains neutral with regard to jurisdictional claims in published maps and institutional affiliations.

**Open Access** This article is licensed under a Creative Commons Attribution-NonCommercial-NoDerivatives 4.0 International License, which permits any non-commercial use, sharing, distribution and reproduction in any medium or format, as long as you give appropriate credit to the original author(s) and the source, provide a link to the Creative Commons licence, and indicate if you modified the licensed material. You do not have permission under this licence to share adapted material derived from this article or parts of it. The images or other third party material in this article are included in the article's Creative Commons licence, unless indicated otherwise in a credit line to the material. If material is not included in the article's Creative Commons licence and your intended use is not permitted by statutory regulation or exceeds the permitted use, you will need to obtain permission directly from the copyright holder. To view a copy of this licence, visit <http://creativecommons.org/licenses/by-nc-nd/4.0/>.

© The Author(s) 2024